Functional expression of a pseudohypoaldosteronism type I mutated epithelial Na^+ channel lacking the pore-forming region of its α subunit

Olivier Bonny,[1] Ahmed Chraibi,[1] Jan Loffing,[2] Nicole Fowler Jaeger,[1] Stefan Gründer,[3] Jean-Daniel Horisberger,[1] and Bernard C. Rossier[1]

[1]Institut de Pharmacologie et de Toxicologie, Université de Lausanne, CH-1005 Lausanne, Switzerland
[2]Institute of Anatomy, University of Zürich, CH-8057 Zürich, Switzerland
[3]University Hospital, Department of Sensory Biophysics, D-72076 Tübingen, Germany

Address correspondence to: Bernard C. Rossier, Institut de Pharmacologie et de Toxicologie, Rue du Bugnon 27, CH-1005 Lausanne, Switzerland. Phone: 41/21-692-5351; Fax: 41/21-692-5355; E-mail: Bernard.Rossier@ipharm.unil.ch.

Received for publication March 16, 1999, and accepted in revised form August 10, 1999.

The autosomal recessive form of type I pseudohypoaldosteronism (PHA-I) is an inherited salt-losing syndrome resulting from diminution-of-function mutations in the 3 subunits of the epithelial Na^+ channel (ENaC). A PHA-I stop mutation ($\alpha_{R508stop}$) of the ENaC α subunit is predicted to lack the second transmembrane domain and the intracellular COOH-terminus, regions of the protein involved in pore function. Nonetheless, we observed a measurable Na^+ current in *Xenopus laevis* oocytes that coexpress the β and γ subunits with the truncated α subunit. The mutant α was coassembled with β and γ subunits and was present at the cell surface at a lower density, consistent with the lower Na^+ current seen in oocytes with the truncated α subunit. The single-channel Na^+ conductance for the mutant channel was only slightly decreased, and the appearance of the macroscopic currents was delayed by 48 hours with respect to wild-type. Our data suggest novel roles for the α subunit in the assembly and targeting of an active channel to the cell surface, and suggest that channel pores consisting of only the β and γ subunits can provide significant residual activity. This activity may be sufficient to explain the absence of a severe pulmonary phenotype in patients with PHA-I.

J. Clin. Invest. **104**:967–974 (1999).

Introduction

Type I pseudohypoaldosteronism (PHA-I) is an inherited disorder that manifests soon after birth and is characterized by failure to thrive, salt wasting, metabolic acidosis, life-threatening hyperkalemia, and dehydration. Despite clinical evidence for hypoaldosteronism, plasma aldosterone and plasma renin activity are elevated, suggesting a defect in aldosterone target tissues. Two kinds of inheritance have been described for PHA-I, with distinct clinical and pathophysiological features (1): the autosomal dominant renal form (OMIM 177735), which was recently linked to mutations in the mineralocorticoid receptor gene (2); and the recessive systemic form (OMIM 264350), which presents with severe Na^+ transport defects in all aldosterone target tissues. It is caused by diminution-of-function mutations in genes encoding the subunits of the amiloride-sensitive epithelial Na^+ channel (ENaC) (3).

ENaC constitutes the rate-limiting step of Na^+ reabsorption through aldosterone-responsive epithelia found in kidneys, colon, salivary and sweat glands, and glucocorticoid-responsive lung epithelia. ENaC is a heteromultimeric protein made of 3 subunits (α, β, and γ), sharing 35% homology at the protein level and the same membrane topology (4). A heterotetrameric structure (αβαγ) has recently been proposed for ENaC (5, 6). It is therefore likely that all cation channels belonging to this gene family are tetrameric, even though a nonameric architecture has been proposed by others (7). Mutagenic studies identified amino acid residues involved in ion permeation and critical for channel block by amiloride in a short segment preceding the second transmembrane domain (the pre-M2 segment) of each of the 3 subunits (8). This demonstrated that all 3 subunits contribute to the formation of the conductive pore. The α subunit plays a specific role in channel assembly and/or targeting to the plasma membrane. This conclusion is based on earlier observations in the *Xenopus* oocyte system showing that only complexes containing the α subunit (α alone or αβ or αγ complexes) are able to form functional channels. When only βγ subunits were present, no detectable amiloride-sensitive current could be measured (4). Taken together, these data suggest that the α subunit contains some specific information needed to get functional channels to the cell surface — information that is lacking in either β or γ subunits.

Homozygous mutations have been identified in all 3 ENaC subunits, causing the recessive form of PHA-I (3). Three mutations in the α subunit have been described: a frameshift (α_{I68fr}), a missense mutation of a conserved cysteine (α_{C133Y}), and a premature stop codon ($\alpha_{R508stop}$). Truncation of the α subunit is predicted to abolish ENaC activity in all tissues because it

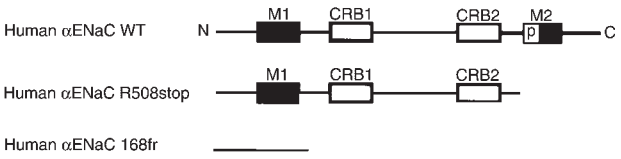

Figure 1
α ENaC subunit truncations reported in recessive PHA-I. Primary structure of wild-type (WT) and predicted deletions of α subunits are illustrated. M1 and M2 denote first and second transmembrane domains; P denotes the pre-M2 domain of the second transmembrane domain. CRB1 and CRB2 stand for cysteine-rich boxes 1 and 2. Both deletion mutations reported for patients with PHA-I (human $\alpha_{R508stop}$ and human α_{I68fr}) predict an interruption of the α subunit before the M2 and the M1 membrane-spanning domains, respectively.

deletes the pore-forming region of the subunit present in at least 2 copies in the channel complex. This prediction is supported by gene disruption of the mouse α gene locus. All αENaC knockout pups present a postnatal lethal pulmonary edema, demonstrating the importance of this subunit in lung liquid clearance at birth (9). By contrast, patients with PHA-I have no neonatal lung phenotype, despite impressive truncations of the α subunit in some kindreds (α_{I68fr} or $\alpha_{R508stop}$). To explain this discrepancy, we considered the following, not mutually exclusive, hypotheses:

(a) Species differences, such as the presence of species-specific channels and subunit or regulatory proteins expressed in the lung, could account for this contradiction. (b) The truncated α subunit may retain some information, leading to some residual activity. This concept is supported by recent in vivo studies demonstrating that less than 20% of ENaC activity in mouse lung is enough to prevent a neonatal lung edema, but not the development of a mild (10) or severe (11) renal phenotype.

To test the latter hypothesis, we introduced the $\alpha_{R508stop}$ mutation in human ENaC and the equivalent $\alpha_{L535stop}$ in rat ENaC, and expressed them in the *Xenopus* oocyte system. We found that when coexpressed with β and γ, the truncated α subunit leads to significant channel activity, although with a delayed time course. If similar activity were present in the lungs of patients with PHA-I carrying such a mutated allele, it might be sufficient to clear their lungs of fluid at birth. This may partially explain the difference in pulmonary phenotype observed between the αENaC-defective mouse and patients with PHA-I, and gives new insights into the comprehension of this disease.

Methods

Site-directed mutagenesis and expression in Xenopus laevis oocytes. Point mutations were introduced into α human ($\alpha_{R508stop}$) and rat ($\alpha_{L535stop}$) ENaC cDNAs by PCR-based mutagenesis. Constructs were checked by sequencing. Capped cRNAs were obtained from linearized cDNAs by in vitro transcription and were injected (3 ng for each subunit) into stage V–VI *X. laevis* oocytes. Oocytes were kept at 19°C in low-Na^+ modified Barth's saline (MBS) (10 mM NaCl, 90 mM NMDG-Cl, 5 mM KCl, 0.41 mM $CaCl_2$, 0.33 mM $CaNO_3$, 0.82 mM $MgSO_4$) supplemented with penicillin (100 U/mL) and streptomycin (100 mg/mL).

Whole-cell current was determined with the 2-electrode voltage-clamp method described previously (4). The amiloride-blockable fraction of the inward current at –100 mV, representative of the ENaC current, was measured as the difference between currents obtained before and after the addition of 100 μM amiloride in solutions containing Na^+ (I_{Na^+}) or Li^+ (I_{Li^+}). Ionic selectivity was assessed as the ratio of amiloride-sensitive macroscopic currents in a bathing solution containing 120 mM of NaCl, LiCl, or KCl. Amiloride sensitivity was determined by blocking channel activity with increasing concentrations of amiloride in 120 mM NaCl at –100 mV.

Binding assay. Measurement of ENaC surface expression was achieved according to Firsov et al. (12), by counting specific binding of $[^{125}I]M_2IgG_1$ (M2Ab) at the surface of oocytes injected with indicated ENaC FLAG-tagged subunits and incubated in low-Na^+ MBS. Anti-FLAG mAb's were purchased from Eastman Kodak Co. (Rochester, New York, USA) and used at a final concentration of 12 nM. Background activity was determined on water- or untagged ENaC–injected oocytes, and was subtracted from values of each condition. The same oocytes were subsequently used for determination of whole-cell Na^+ channel current.

Immunoprecipitation. Oocytes were injected with FLAG-tagged and untagged subunits as specified, and labeled for 12 hours with 1 mCi/mL of $[^{35}S]$methionine in MBS. Microsomal membranes were obtained as described (13) and solubilized in a digitonin (Calbiochem-Novabiochem Corp., San Diego, California, USA) washing buffer (20 mM Tris-HCl [pH 7.5], 100 mM NaCl, 0.5% digitonin, 1 mM phenylmethylsulfonyl fluoride, leupeptin, antipain, pepstatin A). For nondenaturant immunoprecipitations, we used the anti-FLAG M_2IgG_1 mAb (Kodak). A 1:1 mixture of protein G/protein A Sepharose recovered the immunoprecipitates, and these were loaded, after washing, on a 5–8% gradient SDS-PAGE. Denaturant immunoprecipitations were performed with an anti–ratENaC (anti-rENaC) antibody in a 1% TENT solution (50 mM Tris, 5 mM EDTA, 150 mM NaCl, 1% Triton X-100; pH 7.4). Immunoprecipitates were recovered by protein A Sepharose and subjected to electrophoresis. The gels were exposed to XB-1 Kodak film for 2–5 days.

Single-channel recordings. Single-channel recordings were obtained in the cell-attached configuration with a List LM EPC 7 patch-clamp amplifier (List Electronics, Darmstadt, Germany), displayed on an oscilloscope (Tektronix Inc., Heerenveen, the Netherlands) and stored on a digital tape recorder (Biologic Co., Claix, France). Borosilicate glass (Corning Inc., New York, New York, USA) pipettes with a 10- to 20-MΩ resistance, filled with 120 mM LiCl or 120 mM NaCl solutions, were used. The bathing solution was 120 mM KCl

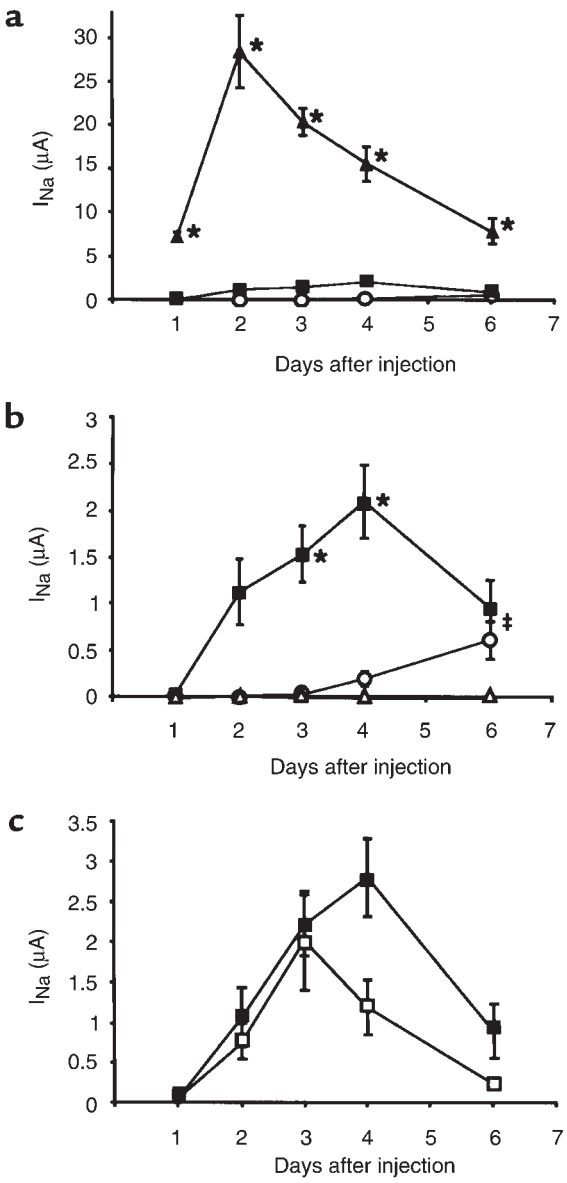

Figure 2

(**a**) Time courses of macroscopic amiloride-sensitive current of wild-type, $\alpha_{L535stop}\beta\gamma$, and $\beta\gamma$ rat ENaC–injected oocytes. Oocytes were injected with 3 ng cRNA of each rat ENaC subunit as follows: $\alpha\beta\gamma$ (filled triangles), $\alpha_{L535stop}\beta\gamma$ (filled squares), or $\beta\gamma$ (open circles). Amiloride-sensitive (100 μM) Na^+ current was determined every day in a bathing solution containing 120 mM NaCl. Oocytes were clamped at –100 mV and measured with the 2-electrode voltage-clamp method. Currents are reported as the mean ± SEM obtained from 17–34 oocytes (6 independent experiments). $^*P < 0.001$, $\alpha\beta\gamma$ channels vs. mutant $\alpha_{L535stop}\beta\gamma$ or $\beta\gamma$ channels. (**b**) Focus on mutant $\alpha_{L535stop}\beta\gamma$ (filled squares) macroscopic current time courses, compared with $\beta\gamma$-injected (open circles) and water-injected (open triangles) oocytes. $^*P < 0.001$, mutant $\alpha_{L535stop}\beta\gamma$ vs. $\beta\gamma$- or water-injected oocytes. $^‡P < 0.001$, mutant $\alpha_{L535stop}\beta\gamma$- and $\beta\gamma$-injected oocytes vs. water-injected oocytes. (**c**) Comparison of human and rat mutant macroscopic current time courses. Human ($\alpha_{R508stop}\beta\gamma$; open squares) and rat ($\alpha_{L535stop}\beta\gamma$; filled squares) ENaC mutants have the same expression pattern over time. No significant difference was detected. Each point represents the mean ± SEM of macroscopic Na^+ channel currents obtained from 15–26 oocytes (4 different batches).

buffered to pH 7.4 with 10 mM Na-HEPES. Single-channel conductances for Na^+ and Li^+ were calculated from current/voltage relationships between –150 and +10 mV. Current signals were filtered at 200 Hz with an 8-pole Bessel filter (Frequency Devices Inc., Haverhill, Massachusetts, USA) and digitized at 1 kHz using a Labmaster analog-digital interface and Fetchex software (Axon Instruments Inc., Foster City, California, USA).

Immunofluorescence assay. Four days after injection, oocytes were fixed with 3% paraformaldehyde (Merck KGaA, Darmstadt, Germany) in PBS for 4 hours at 4°C. For immunochemistry, the tyramide signal amplification kit (TSA-Direct; NEN Life Science Products Inc., Boston, Massachusetts, USA) was used. Cryosections (6-μm thick) were incubated for 1 hour with a 1:100 diluted anti-FLAG IgG antibody (Kodak). After washings, they were incubated for 1 hour with a 1:100 dilution of a horseradish peroxidase–conjugated sheep anti-mouse immunoglobulin (Amersham Pharmacia Biotech AB, Uppsala, Sweden), subsequently revealed by incubation for 10 minutes with the provided fluorescein-tyramide conjugates diluted 1:50. To label the F-actin cytoskeleton of the oocyte plasma membrane, a 1:50 dilution of rhodamine-conjugated phalloidin (Molecular Probes Inc., Eugene, Oregon, USA) was added to the amplification buffer. Sections were mounted with DAKO-Glycergel (DAKO Corp., Glostrup, Denmark) containing 2.5% of 1,4-diazabicyclo[2.2.2]octane as a fading retardant (Sigma Chemical Co., Buchs, Switzerland) and were studied by epifluorescence with a Polyvar microscope (Reichert-Jung, Vienna, Austria). Digitized images were acquired with a VISICAM CCD camera (Visitron, Puchheim, Germany) and processed by Image-Pro Plus software (version 3.0; Media Cybernetics, Silver Spring, Maryland, USA). Identical settings were used for each oocyte.

Results

The rat and human αENaC stop mutations allow significant expression of active channels. The stop mutation ($\alpha_{R508stop}$) found in patients with PHA-I interrupts the αENaC protein 46 amino acids before the predicted α-helix of the second transmembrane domain (M2), deleting this domain, the domain preceding M2 (pre-M2), and the intracellular COOH-terminus. It does, however, conserve a large portion of the extracellular loop and the 2 cysteine-rich boxes, characteristic of the ENaC gene superfamily (14) (Figure 1). We introduced the stop mutation in the rat αENaC subunit at the equivalent residue ($\alpha_{L535stop}$) and coexpressed it with β and γ rat ENaC. When measured with the 2-electrode voltage-clamp method, reproducible amiloride-sensitive currents were recorded from $\alpha_{L535stop}\beta\gamma$-injected oocytes, reaching 13% of currents measured in $\alpha\beta\gamma$-injected oocytes 4 days after injection (Figure 2, a–c). These currents were significantly higher than those recorded in oocytes injected with $\beta\gamma$ subunits alone ($P < 0.001$ at days 3 and 4 after injection) or with water ($P < 0.001$ at days 3–6) (Figure 2b). Three different kinetics for the appearance of macroscopic amiloride-sensitive Na^+ cur-

Table 1
Macroscopic current characteristics of rat and human ENaC expressed in *Xenopus* oocytes

Species	Injected subunits	Amiloride sensitivity			Current ratio				Day of maximal current during time course
		$K_{i\ amiloride}$ (μM)	*n*	I_{Na^+} (μA)[C]	I_{Li^+}/I_{Na^+}	I_{Na^+}/I_{K^+}	*n*	I_{Na^+} (μA)[C]	
Rat	αβγ	0.22 ± 0.01	34	10.3	1.7 ± 0.1	>50	20	5.9	Day 2
	$\alpha_{L535stop}\beta\gamma$	5.97 ± 0.38[A,B]	45	1.4	1.0 ± 0.1[A]	>50	33	0.9	Day 4
	βγ	2.38 ± 0.72[A]	15	1.8	0.9 ± 0.1[A]	21[A]	12	2.6	> Day 6
	αβ	1.38 ± 0.11[A]	15	4.0	0.7 ± 0.1[A]	>50	12	4.0	Day 4
	αγ	0.17 ± 0.02	14	0.6	1.4 ± 0.1	>50	12	0.8	Day 4
Human	αβγ	0.16 ± 0.02	21	16.4	1.3 ± 0.1	>50	18	28.1	Day 2
	$\alpha_{R535stop}\beta\gamma$	0.16 ± 0.04	22	2.8	1.4 ± 0.1	>50	26	2.2	Day 3
	αβ	0.05 ± 0.02	3	0.3	1.6 ± 0.2	>50	8	2.8	ND
	αγ	0.08 ± 0.01	14	4.8	1.3 ± 0.1	>50	16	3.8	ND

[A]$P < 0.001$ vs. wild-type channels. [B]$P < 0.001$ vs. βγ channels. [C]Mean maximal I_{Na^+} current in this set of experiments. ND, not determined.

rent could be observed during the postinjection period (Figure 2, a and b). (a) In αβγ rENaC-injected oocytes, amiloride-sensitive currents were already detectable after a few hours, and reached their peak on the second day after injection. (b) Oocytes injected with $\alpha_{L535stop}\beta\gamma$ display slower kinetics, reaching their peak after 4 days. (c) Surprisingly, amiloride-sensitive currents were recorded from oocytes injected with βγ rENaC (between 0.5 and 2 μA) 6 days after injection (significantly higher than water-injected oocytes; $P < 0.001$). Their maximal expression was recorded at the seventh day.

To assess putative species difference in the expression of this mutant, as related in vivo between humans and mice, we studied the human $\alpha_{R508stop}$ mutation. When coinjected with human β and γ ENaC, the $\alpha_{R508stop}$ led to similar amiloride-sensitive current expression as the rat mutant $\alpha_{L535stop}\beta\gamma$ (Figure 2c). Both mutants had the same time course, with a delayed peak of activity compared with wild-type channels. Human βγ currents were significantly smaller than the $\alpha_{R508stop}\beta\gamma$ currents, but significantly higher than water-injected oocytes, at day 3 after injection (data not shown).

Differences in macroscopic current properties between human and rat channels. Because the second transmembrane domain forms the channel pore and participates in the selectivity filter and amiloride sensitivity (8), we characterized the macroscopic currents resulting from coinjection of human $\alpha_{R508stop}$ and rat $\alpha_{L535stop}$ with their respective β and γ subunits. They demonstrated subtle differences (Table 1). Human $\alpha_{R508stop}\beta\gamma$ channels had similar amiloride sensitivity ($K_{i\ amiloride}$ = 0.16 ± 0.04 μM) and ionic selectivity, determined as Li^+/Na^+ or Na^+/K^+ amiloride–sensitive current ratio (I_{Li^+}/I_{Na^+} = 1.4 ± 0.1; I_{Na^+}/I_{K^+} > 50), as human wild-type channels. By contrast, rat $\alpha_{L535stop}\beta\gamma$ channels had a lower amiloride sensitivity than wild-type channels ($K_{i\ amiloride}$ = 5.97 ± 0.38 μM; $P < 0.001$), and lost Li^+/Na^+ selectivity (I_{Li^+}/I_{Na^+} = 1.0 ± 0.1; $P < 0.001$). But they conserved selectivity for Na^+ over K^+ (I_{Na^+}/I_{K^+} > 50). Currents from oocytes injected with rat βγ ENaC displayed characteristics close to those of rat $\alpha_{L535stop}\beta\gamma$. Amiloride sensitivity was, however, slightly higher ($K_{i\ amiloride}$ = 2.38 ± 0.72 μM; $P < 0.001$) compared with mutant $\alpha_{L535stop}\beta\gamma$. Selectivity for Na^+ over K^+ was statistically different from wild-type, but remained high (I_{Na^+}/I_{K^+} = 21; $P < 0.001$). Unfortunately, we have not been able to perform similar studies on human βγ channels because currents were too low.

As reported previously (15), rat αβ and αγ channels have different macroscopic characteristics (Table 1): αγ channels resemble wild-type channels, whereas αβ channels demonstrate amiloride resistance and a loss of Li^+/Na^+ selectivity. By contrast, human αβ and αγ channels displayed the same amiloride sensitivity (αβ: $K_{i\ amiloride}$ = 0.05 ± 0.02 μM; and αγ: $K_{i\ amiloride}$ = 0.08 ± 0.01 μM) and selectivity (αβ: I_{Li^+}/I_{Na^+} = 1.6 ± 0.2, I_{Na^+}/I_{K^+} > 50; and αγ: I_{Li^+}/I_{Na^+} = 1.3 ± 0.1, I_{Na^+}/I_{K^+} > 50) as human wild-type channels, thus confirming species differences depending on subunit arrangements.

In summary, although some features were distinct to either the human or the rat Na^+ mutant channel, the important and common feature for both species is that a surprisingly large, macroscopic amiloride-sensitive current was observed, presenting the same delayed kinetics in both species. Subsequent studies were performed on the rat channel, for which more information concerning cell-surface expression is available (12).

The diminution of expressed activity of the mutated channel is due to a decreased number of channels at the cell surface. Whole-cell Na^+ current can be summarized by the following equation:

(Equation 1)

$$I = g_{Na}\ N\ P_o\ (E - E_{Na})$$

where g_{Na} is the single-channel conductance for Na^+, N is the total number of channels for a given cell, P_o is the mean open probability for a single channel, E is the membrane potential, and E_{Na} is the reverse potential for Na^+ (16). The driving force for Na^+ ions ($E - E_{Na}$) was kept approximately constant by clamping the oocyte membrane potential at –100 mV, and cannot account for the observed decreased mutant channel current. To deter-

mine conductance and P_o, single-channel recordings were obtained 4 days after injection in the cell-attached patch configuration from $\alpha_{L535stop}\beta\gamma$-injected oocytes. Single-channel conductances determined between –150 and +10 mV were 4.03 ± 0.26 pS (n = 12) with Na^+ in the pipette, and 5.08 ± 0.07 pS (n = 8) in the presence of Li^+. They were both slightly lower than values given for the wild-type ENaC, but this difference could not explain the diminution of macroscopic current. The low Li^+ conductance confirmed the relative loss of selectivity for Li^+ compared with Na^+ observed in macroscopic current experiments. As described by others (17), P_o was highly variable and no obvious difference was observed. We addressed the question of the number of channels at the cell surface by a binding assay, described previously (12). Oocytes were injected with $\alpha\beta_{FLAG}\gamma_{FLAG}$, $\alpha_{L535stop}\beta_{FLAG}\gamma_{FLAG}$, or $\beta_{FLAG}\gamma_{FLAG}$. Binding assays with iodinated anti-FLAG antibodies were performed daily during 4 days. The number of mutant channels detected at the cell surface was rising as late as 4 days after injection (Figure 3a). At this day, they reached a highly significant binding level over βγ-injected oocytes. The number of detected channels at the cell surface paralleled the appearance of the Na^+ channel current (Figure 3b), leading to a constant binding/current ratio (Figure 3c). This indicates that the number of mutant channels at the cell surface was decreased in parallel to the decrease of I_{Na^+}. This can also be illustrated by plotting binding versus I_{Na^+} (Figure 3d). A linear relationship existed between the number of channels at the cell surface (reported as binding per oocyte) and the macroscopic amiloride-sensitive Na^+ current for both mutant and wild-type channels, but the slopes of the regression lines were not significantly different. These results indicate that the observed $\alpha_{L535stop}\beta\gamma$ current reduction is mainly due to a proportional decrease of the channel number at the cell surface.

The decreased number of channels at the cell surface is due to a retention of channel proteins in intracellular compartments. To observe the subcellular distribution of wild-type and mutant channels, we used immunofluorescence to detect the localization of epitope-tagged subunits in cryosections of oocytes that were injected with either water, $\alpha\beta_{FLAG}\gamma_{FLAG}$, $\alpha_{L535stop}\beta_{FLAG}\gamma_{FLAG}$, or $\beta_{FLAG}\gamma_{FLAG}$. Oocytes injected with $\alpha\beta_{FLAG}\gamma_{FLAG}$ exhibited a bright immunofluorescent signal at the circumference of the oocyte and a weaker staining in the intracellular compartment (Figure 4b). Higher magnification and costaining of the actin cytoskeleton, which is highly abundant in the microvilli of the cell surface, confirmed that the immunofluorescence at the periphery of the oocyte represents FLAG-tagged ENaC subunits present at the cell surface (Figure 4, f and j). Oocytes expressing $\alpha_{L535stop}\beta_{FLAG}\gamma_{FLAG}$ exhibited only a weak signal in the plasma membrane, but the

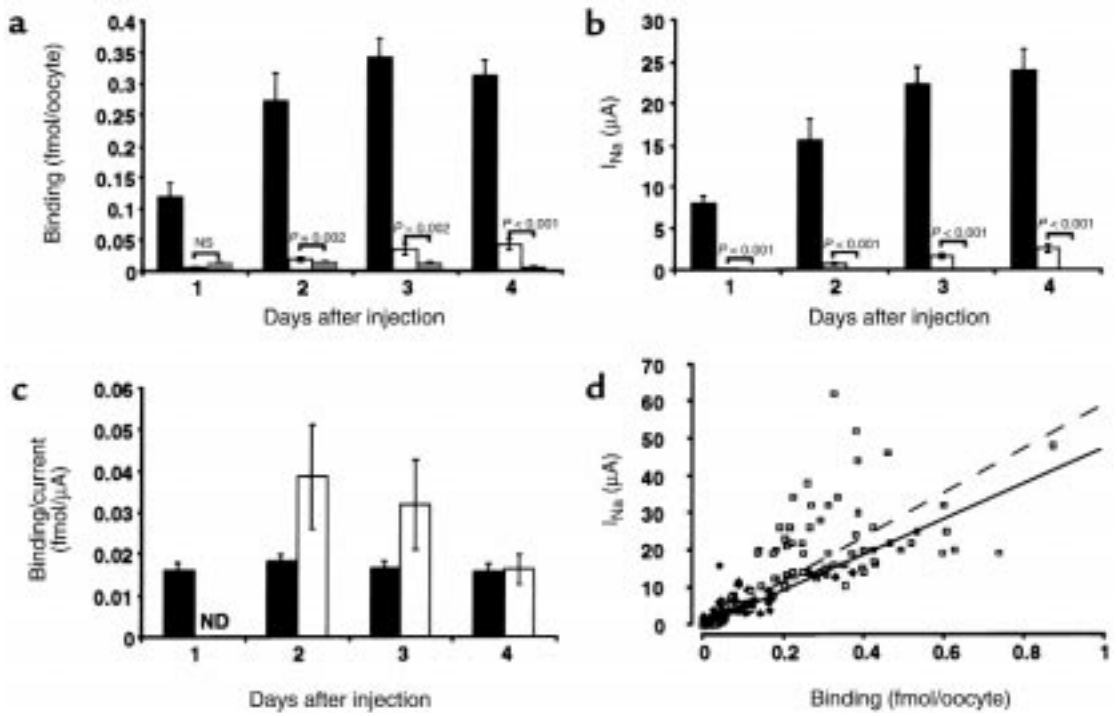

Figure 3

(**a**) Quantitative determination of the number of channel molecules present at the cell surface. Epitope-tagged β_{FLAG} and γ_{FLAG} rENaC subunits were coinjected with α wild-type (filled bars), $\alpha_{L535stop}$ (open bars), or water (gray bars) in *Xenopus* oocytes. Values are mean ± SEM of 2 different experiments with 12 oocytes per experiment and per condition. *P* values of unpaired Student's *t* test are indicated. (**b**) Whole-cell amiloride-sensitive Na^+ currents. βγ channel currents are undetectable. (**c**) Ratio of the bound anti-FLAG IgG (binding; **a**) to the whole-cell Na^+ current (**b**) for αβγ and mutant $\alpha_{L535stop}\beta\gamma$ channels. ND, not determined. (**d**) Representation of binding values plotted against I_{Na^+}. The slopes of the linear regression curves are not statistically different ($y = 59x$, $r^2 = 0.44$ for αβγ channels [open squares and dashed line]; and $y = 48x$, $r^2 = 0.54$ for the mutant channel $\alpha_{L535stop}\beta\gamma$ [filled diamonds and solid line].

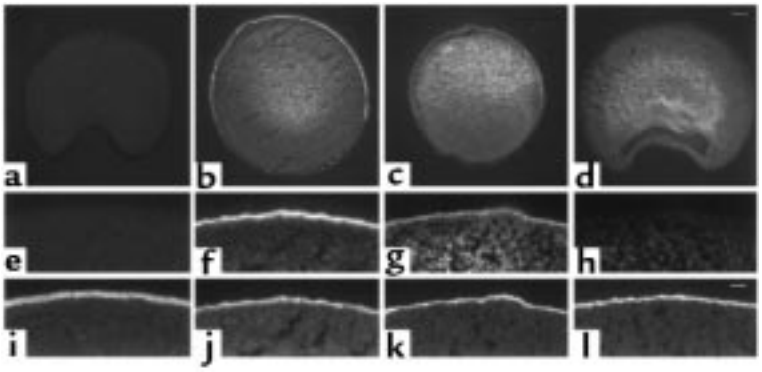

Figure 4
Immunofluorescence of oocytes injected either with $\alpha\beta_{FLAG}\gamma_{FLAG}$ (**b**, **f**, and **j**), $\alpha_{L535stop}\beta_{FLAG}\gamma_{FLAG}$ (**c**, **g**, and **k**), $\beta_{FLAG}\gamma_{FLAG}$ (**d**, **h,** and **l**), or water (**a**, **e,** and **i**). Detection of FLAG-tagged ENaC subunits with an anti-FLAG mAb (**a**–**h**), and of the microvilli actin cytoskeleton with rhodamine-conjugated phalloidin (**i**–**l**). (**a**–**d**) Low-power magnifications; scale bar in **d**: 100 μm. (**e**–**l**) High-power magnifications; scale bar in **l**: 20 μm.

intracellular staining was clearly increased, indicating a retention of channels in an intracellular compartment (Figure 4, c, g, and k). $\alpha_{L535stop}\beta_{FLAG}\gamma_{FLAG}$ was, like $\alpha\beta_{FLAG}\gamma_{FLAG}$, predominantly found at the vegetal pole of the oocyte (Figure 4, b and c), suggesting that the trafficking of $\alpha_{L535stop}\beta_{FLAG}\gamma_{FLAG}$ to the cell surface, although less efficient, obeys the same rules as that of $\alpha\beta_{FLAG}\gamma_{FLAG}$. In oocytes expressing $\beta_{FLAG}\gamma_{FLAG}$ (Figure 4, d, h, and l), no ENaC-related plasma membrane staining was observed 4 days after injection; FLAG-tagged ENaC subunits were exclusively found in intracellular compartments. In water-injected oocytes (Figure 4, a, e, and i), no immunofluorescent signal for ENaC was observed. Actin cytoskeleton was stained as in the other groups of oocytes.

In addition to the slower appearance and/or the faster retrieval of the mutant channel at the cell surface, the decreased channel number could be due to an early degradation of the channel complex (shorter half-life), a misassembly of the 3 subunits, a mistrafficking, or a combination of any of these possibilities.

The faithful translation of the protein (wild-type or truncated) can be assessed by a denaturant immunoprecipitation assay (Figure 5a). Using an anti-rat αENaC antibody, we were able to efficiently immunoprecipitate both rat and human αENaC subunits. This experiment showed efficient translation of both mutant proteins. Importantly, no evidence for a significant read-through of the translational stop codon was detected (Figure 5a). No early degradation of the mutant complex or difference in protein turnover could be demonstrated by pulse-chase experiments (not shown).

Assembly of $\alpha_{L535stop}$ with β and γ subunits was assessed by nondenaturant immunoprecipitation of microsomal membranes prepared from [^{35}S]methionine-labeled ENaC-injected oocytes. Figure 5b shows an autoradiogram of an SDS-polyacrylamide gel, demonstrating assembly of the FLAG-tagged $\alpha_{L535stop}$ together with β and γ ENaC subunits (lane 2). Specificity of the assembly was assessed by changing the FLAG-tagged subunit of this complex (lane 3). The γ FLAG-tagged subunit was also able to coimmunoprecipitate the $\alpha_{L535stop}$ with the β subunit. Specificity of the antibody is demonstrated on lanes 4 and 6, where nontagged mutant subunits and water-injected oocytes were used, respectively. Finally, the specificity of the coimmunoprecipitation is demonstrated by oocytes injected with βγ (lane 5), in which the 2 proteins are coassembled. These results indicate that the mutated $\alpha_{L535stop}$ subunit coassembles with β and γ, despite the deletion of its second transmembrane domain and the COOH-terminal intracellular tail.

To assess the presence of all 3 subunits at the cell surface, we also used the binding assay with epitope-tagged subunits. Three days after injection, binding signal for oocytes injected with $\alpha_{L535stopFLAG}\beta\gamma$ was in the same range as that for oocytes injected with $\alpha_{L535stop}\beta_{FLAG}\gamma_{FLAG}$, and the amiloride-sensitive currents were identical (Figure 6). Together with the results from the binding assay (Figure 3a) and the coimmunoprecipitation assay (Figure 5b), our data indicate that the 3 ENaC subunits are present at the cell surface and coassembled to form an active channel.

Discussion

Assembly domain and targeting signal of the α subunit. The 3 subunits of the mutated channel ($\alpha_{L535stop}$, β, and γ) are coassembled, suggesting that the second transmembrane domain (M2) and the COOH-terminal part of αENaC subunit are not necessarily required for assembly. This is in agreement with previous experiments performed on the γ subunit (18). We propose here that an assembly domain is present in the first 535 residues of the α subunit.

Measurable currents were observed after injection of $\alpha_{L535stop}\beta\gamma$ or βγ in *X. laevis* oocytes. These currents could be due to the preferential association of the injected β and γ subunits with an endogenous subunit. Despite some evidence for endogenous amiloride-sensitive currents (19), to date, no significant endogenous expression of ENaC subunits have been identified in *Xenopus* oocytes.

The 3 coassembled subunits ($\alpha_{L535stop}$, β, and γ) were detected at the cell surface of the oocyte by the antibody-binding assay, although with a decreased density. This indicates that a significant part of mutated channels reaches the plasma membrane. This impaired trafficking or faster retrieval results in a delayed appearance and a decreased number of channels at the cell surface (proportional to the decrease in amiloride-sensitive macroscopic current). The mechanisms by

which ENaC is targeted to the plasma membrane are not known. In the oocyte, the α subunit can reach the cell membrane on its own, as well as in complexes containing α (αβ and αγ), but to a lesser extent compared with complexes containing all 3 subunits (αβγ) (4). The importance of α for the targeting of ENaC complexes to the cell surface is highlighted by the kinetics of macroscopic currents studied in the postinjection period. Comparison of kinetics of βγ subunits coinjected alone or coinjected with the truncated $\alpha_{L535stop}$ or with the full-length αENaC showed a rapid and efficient trafficking with the wild-type αENaC, a short delay and a decrease in the number of channels reaching the surface with the truncated $\alpha_{L535stop}$, and a long delay and a decreased number of channels when no α subunit was present. This suggests that trafficking signals are contained in the α subunit in at least 2 positions, 1 before and 1 after amino acid 535. In a previous study (20), a proline-rich domain in the intracellular COOH-terminal part of the α subunit was identified as interacting with the SH3 domain of α-spectrin, a component of the cytoskeleton. This proline-rich domain could target the wild-type ENaC complex to the apical cell surface. Its deletion in the $\alpha_{L535stop}$ mutation could account for the disturbed trafficking. We therefore propose that the first 535 residues of αENaC contain enough sorting information to permit a trafficking of βγ subunits to the cell surface, yet with a slower time course. The reduction in the number of channels at the cell surface is enough to account for the observed diminution of the I_{Na^+}. Thus, the mutant $\alpha_{L535stop}$ coexpressed with β and γ in the *Xenopus* oocyte gives rise to functional channels with a Na^+ conductance close to wild-type ENaC. This raises an intriguing question about the structure of the pore of $\alpha_{L535stop}\beta\gamma$ channels.

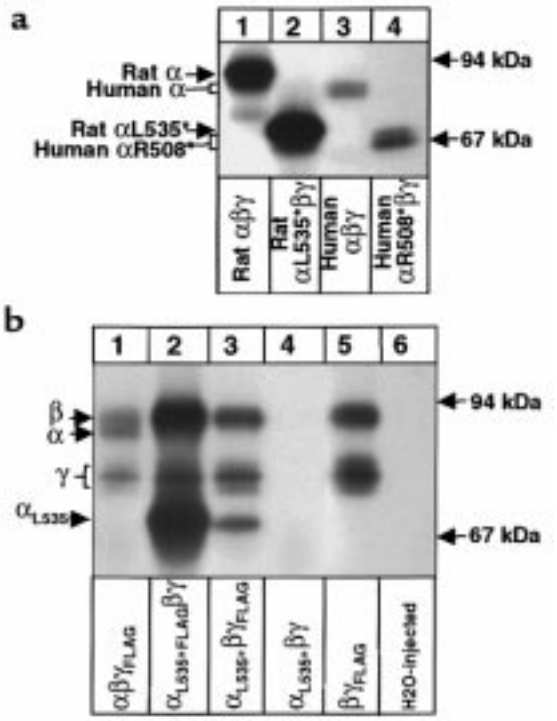

Figure 5
(**a**) Denaturant immunoprecipitation with an anti-rat αENaC antibody. Oocytes were injected with rat wild-type αβγ (lane 1), rat $\alpha_{L535stop}\beta\gamma$ (lane 2), human wild-type αβγ (lane 3), or human $\alpha_{R508stop}\beta\gamma$ (lane 4) and were metabolically labeled. Equal counts of microsomal preparation were subjected to immunoprecipitation by a rat anti-α antibody. Recovered immunoprecipitates were run on a 5–8% SDS-polyacrylamide gel. Molecular weight is indicated. (**b**) Nondenaturant coimmunoprecipitation of wild-type and mutant rENaC. Oocytes were injected with γ_{FLAG} subunits (lanes 1, 3, and 5), with $\alpha_{L535stopFLAG}$ subunit (lane 2), or without FLAG subunit (lanes 4 and 6), coinjected with wild-type rENaC or mutant $\alpha_{L535stop}$ subunits, as indicated. Nondenaturant coimmunoprecipitation was performed with an anti-FLAG mAb. Specificity of the antibody is demonstrated on lanes 4 and 6 (no FLAG-tagged subunits injected). Specificity of the coimmunoprecipitation is demonstrated on lanes 2, 3, and 5 (no α subunit injected).

The rat $\alpha_{L535stop}\beta\gamma$ channel presents a 27-fold decreased sensitivity to amiloride and a loss of selectivity of Li^+ over Na^+. It is remarkable that a complete deletion of the pre-M2 and M2 domains of the α subunit ($\alpha_{L535stop}$) causes changes in channel properties nearly identical to those observed previously with point mutations (α_{S583C}) (8) or chimeric constructs (21). Rat $\alpha_{L535stop}\beta\gamma$ channels have the same macroscopic characteristics (amiloride resistance and Li^+ loss of selectivity) as βγ channels, except for 2 relatively small quantitative differences (amiloride sensitivity and K^+ selectivity). Overall, the resemblance between currents obtained from $\alpha_{L535stop}\beta\gamma$ and βγ channels is striking. We would like to propose a model wherein the pore is made by pre-M2 and M2 domains from βγ subunits only.

Functional role of $\alpha_{L535stop}\beta\gamma$ channels in PHA-I phenotype. Disruption of the α subunit results in 2 different phenotypes, depending on whether the disruption is in humans (patients with PHA-I) or in mice (knockout experiment). In mice, α knockout pups die within 40 hours after birth, mainly from an inability to clear their lungs of fluid (9). No residual ENaC activity could be recorded in these animals. This pulmonary phenotype can be rescued by low levels of ENaC activity in the mouse lung (<20%), as recently reported for disruption of the γ (11) and β (10) subunits and for an α knockout mouse rescued by a transgenic rat α subunit (22). Thus, a low level of ENaC activity seems to be sufficient in vivo to rescue the pulmonary phenotype. In humans, no neonatal pulmonary phenotype was described for patients with PHA-I, but clinical evidence for light pulmonary symptoms arises from careful examination of young patients (23–25). These patients present early respiratory events such as wheezing or recurrent viral infections and, in 1 case, recurrent *Pseudomonas* infections (26). Our data suggest that the channel activity measured in vitro could be sufficient in vivo to explain the absence of neonatal pulmonary symptoms in patients with PHA-I suffering from the $\alpha_{R508stop}$ mutation. For the more severe truncations, this explanation may not be suffi-

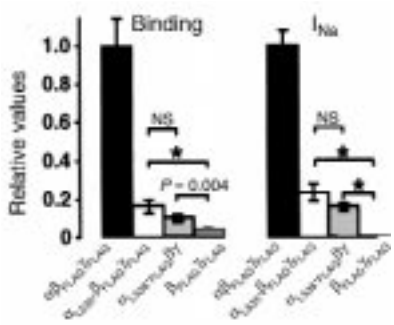

Figure 6
Cell-surface detection of FLAG-tagged subunits. Oocytes were injected with $\alpha\beta_{FLAG}\gamma_{FLAG}$ (filled bars), $\alpha_{L535stop}\beta_{FLAG}\gamma_{FLAG}$ (open bars), $\alpha_{L535stopFLAG}\beta\gamma$ (light gray bars), or $\beta_{FLAG}\gamma_{FLAG}$ (dark gray bars). After 3 days of incubation, binding assay was performed, and the number of FLAG-tagged molecules present at the cell surface was determined. Values represent the means of 24 oocytes ± SEM (2 batches). Unpaired *t* test was used when indicated (*$P < 0.001$). NS, not significant.

cient. The shorter truncation described in PHA-I kindred, α_{I68fr} (Figure 1), leads to a protein of 143 residues with a deletion of most of the α subunit, leaving only the NH_2-terminus. When expressed in the oocyte in association with human β and γ subunits, amiloride-sensitive currents are very low (0.1% of wild-type αβγ) (27). Thus, 2 truncations of different lengths of the α subunit lead in vivo to the same renal phenotype in humans, despite a 100-fold difference in their expression in the oocyte system. Whether such a low residual activity observed in vitro would be enough to prevent a lung phenotype in vivo remains to be seen. Species-specific factors may have an additional role to explain the phenotype difference between mice and humans. In addition, the oocyte expression system may lack specific renal factors that could modulate the expression of the channel. Expression of wild-type and mutated channels in the highly differentiated cortical collecting duct principal cell line (28), or expression of α_{I68fr} or $\alpha_{L535stop}$ mutations in mice by homologous recombination, should help in resolving these issues.

Acknowledgments

We thank M. Lazdunsky for the generous gift of the human αβγ ENaC cDNA, and M. Robert-Nicoud, S. Kohler, and P. Greasley for help in the elaboration of the manuscript. Many thanks to L. Schild, D. Firsov, and D. Bertrand for helpful discussions, and to N. Skarda-Coderey for secretarial help. O. Bonny is supported by a grant from the Swiss National Science Foundation (31-48141.96, M.D.-Ph.D. program of the Swiss Academy of Medical Sciences). B.C. Rossier is also supported by a grant from the Swiss National Science Foundation (31-43384.95).

1. Hanukoglu, A. 1991. Type I pseudohypoaldosteronism includes two clinically and genetically distinct entities with either renal or multiple target organ defects. *J. Clin. Endocrinol. Metab.* **73**:936–944.
2. Geller, D.S., et al. 1998. Mutations in the mineralocorticoid receptor gene cause autosomal dominant pseudohypoaldosteronism type I. *Nat. Genet.* **19**:279–281.
3. Rossier, B.C. 1997. 1996 Homer Smith Award Lecture. *Cum grano salis*: the epithelial sodium channel and the control of blood pressure. *J. Am. Soc. Nephrol.* **8**:980–992.
4. Canessa, C.M., et al. 1994. Amiloride-sensitive epithelial Na^+ channel is made of three homologous subunits. *Nature.* **367**:463–467.
5. Firsov, D., Gautschi, I., Merillat, A.M., Rossier, B.C., and Schild, L. 1998. The heterotetrameric architecture of the epithelial sodium channel. *EMBO J.* **17**:344–352.
6. Kosari, F., et al. 1998. Subunit stoichiometry of the epithelial sodium channel. *J. Biol. Chem.* **273**:13469–13474.
7. Snyder, P.M., Cheng, C., Prince, L.S., Rogers, J.C., and Welsh, M.J. 1998. Electrophysiological and biochemical evidence that DEG/ENaC cation channels are composed of nine subunits. *J. Biol. Chem.* **273**:681–684.
8. Schild, L., Schneeberger, E., Gautschi, I., and Firsov, D. 1997. Identification of amino acid residues in the alpha, beta, and gamma subunits of the epithelial sodium channel involved in amiloride block and ion permeation. *J. Gen. Physiol.* **109**:15–26.
9. Hummler, E., et al. 1996. Early death due to defective neonatal lung liquid clearance in alpha-ENaC–deficient mice. *Nat. Genet.* **12**:325–328.
10. Pradervand, S., et al. 1999. Salt restriction induces pseudohypoaldosteronism type 1 in mice expressing low levels of the beta-subunit of the amiloride-sensitive epithelial sodium channel. *Proc. Natl. Acad. Sci. USA.* **96**:1732–1737.
11. Barker, P.M., et al. 1998. Role of gamma ENaC subunit in lung liquid clearance and electrolyte balance in newborn mice. Insights into perinatal adaptation and pseudohypoaldosteronism. *J. Clin. Invest.* **102**:1634–1640.
12. Firsov, D., et al. 1996. Cell surface expression of the epithelial Na channel and a mutant causing Liddle syndrome: a quantitative approach. *Proc. Natl. Acad. Sci. USA.* **93**:15370–15375.
13. Geering, K., Theulaz, I., Verrey, F., Hauptle, M.T., and Rossier, B.C. 1989. A role for the beta-subunit in the expression of functional Na^+-K^+-ATPase in *Xenopus* oocytes. *Am. J. Physiol.* **257**:C851–C858.
14. Firsov, D., Robert-Nicoud, M., Gruender, S., Schild, L., and Rossier, B.C. 1999. Mutational analysis of cysteine-rich domains of the epithelium sodium channel. Identification of cysteines essential for channel expression at the cell surface. *J. Biol. Chem.* **274**:2743–2749.
15. McNicholas, C.M., and Canessa, C.M. 1997. Diversity of channels generated by different combinations of epithelial sodium channel subunits. *J. Gen. Physiol.* **109**:681–692.
16. Hille, B. 1992. *Ionic channels of excitable membranes.* Sinauer Associates Inc. Sunderland, MA. 1–20.
17. Palmer, L.G., and Frindt, G. 1988. Conductance and gating of epithelial Na channels from rat cortical collecting tubule. Effects of luminal Na and Li. *J. Gen. Physiol.* **92**:121–138.
18. Adams, C.M., Snyder, P.M., and Welsh, M.J. 1997. Interactions between subunits of the human epithelial sodium channel. *J. Biol. Chem.* **272**:27295–27300.
19. Weber, W.M., Liebold, K.M., and Clauss, W. 1995. Amiloride-sensitive Na^+ conductance in native *Xenopus* oocytes. *Biochim. Biophys. Acta.* **1239**:201–206.
20. Rotin, D., et al. 1994. An SH3 binding region in the epithelial Na+ channel (alpha rENaC) mediates its localization at the apical membrane. *EMBO J.* **13**:4440–4450.
21. Waldmann, R., Champigny, G., and Lazdunski, M. 1995. Functional degenerin-containing chimeras identify residues essential for amiloride-sensitive Na^+ channel function. *J. Biol. Chem.* **270**:11735–11737.
22. Hummler, E., et al. 1997. A mouse model for the renal salt-wasting syndrome pseudohypoaldosteronism. *Proc. Natl. Acad. Sci. USA.* **94**:11710–11715.
23. Kerem, E., et al. 1997. Respiratory disease in patients with the systemic form of pseudohypoaldosteronism type I. *Pediatr. Pulmonol. Suppl.* **14**:78–79. (Abstr.)
24. Hogg, R.J., Marks, J.F., Marver, D., and Frolich, J.C. 1991. Long term observations in a patient with pseudohypoaldosteronism. *Pediatr. Nephrol.* **5**:205–210.
25. Hanukoglu, A., Bistritzer, T., Rakover, Y., and Mandelberg, A. 1994. Pseudohypoaldosteronism with increased sweat and saliva electrolyte values and frequent lower respiratory tract infections mimicking cystic fibrosis. *J. Pediatr.* **125**:752–755.
26. Marthinsen, L., et al. 1998. Recurrent Pseudomonas bronchopneumonia and other symptoms as in cystic fibrosis in a child with type I pseudohypoaldosteronism. *Acta Paediatr.* **87**:472–474.
27. Bonny, O., Rossier, B.C., and Hummler, E. 1997. Functional analysis of human alpha ENaC mutation (I68fr) causing PHA-1. *J. Am. Soc. Nephrol.* **8**:M572. (Abstr.).
28. Bens, M., et al. 1999. Corticosteroid-dependent sodium transport in a novel immortalized mouse collecting duct principal cell line. *J. Am. Soc. Nephrol.* **10**:923–934.